Anal Bioanal Chem (2010) 398:2351–2362
DOI 10.1007/s00216-010-4037-5

REVIEW

Trends in solid-state NMR spectroscopy and their relevance for bioanalytics

Silvia Paasch · Eike Brunner

Received: 20 April 2010 / Revised: 14 June 2010 / Accepted: 14 July 2010 / Published online: 14 August 2010

Abstract Based on continuous methodical advances and developments, solid-state NMR spectroscopy has become a powerful tool for the investigation of various materials, including polymers, glasses, zeolites, fullerenes, and many others. During the past decade, solid-state NMR spectroscopy also found increasing interest for the study of biomolecules. For example, membrane proteins reconstituted into lipid environments such as bilayers or vesicles, protein aggregates such as amyloid fibrils, as well as carbohydrates can now be studied by solid-state NMR spectroscopy. This review briefly introduces the principles of solid-state NMR spectroscopy and highlights novel methodical trends. Selected applications demonstrate the possibilities of solid-state NMR spectroscopy as a valuable bioanalytical tool.

Keywords Bioanalytics · Nuclear magnetic resonance · Solid state · Biomolecules

Introduction

Bioanalytics deals with the detection and characterization of proteins, nucleic acids, carbohydrates, and lipids. Liquid-state nuclear magnetic resonance (NMR) spectroscopy has become one of the most successful techniques for investigations of the structure and dynamics of biomolecules in solution [1, 2]. During the past decade, solid-state NMR spectroscopy found an increasing number of biological applications, for example, the study of membrane proteins in lipid environments (see Fig. 1), protein aggregates such as amyloid fibrils, as well as crystalline proteins or protein precipitates [3–22]. Biomineralization phenomena can be studied by solid-state NMR spectroscopy as well [23], including investigations on integral cells [24].

In special cases, conventional one-dimensional NMR spectroscopy allows the detection and characterization of certain biomolecules. A recent example is shown in Fig. 2. Unexpectedly, chitin-based scaffolds could be identified for the first time in the skeleton of the marine demosponge *Ianthella basta* by solid-state ^{13}C NMR spectroscopy [25]. Similar scaffold structures were also observed and characterized by solid-state NMR spectroscopy in diatom cell walls [26]. The biopolymer chitin exhibits a rather simple and well-known ^{13}C NMR spectrum; hence, the identification of the spectral fingerprint can be solely based on one-dimensional NMR spectroscopy. In most cases, however, multidimensional NMR techniques must be applied in analogy to liquid-state NMR spectroscopy to resolve the various signals and to extract structural information from the spectra. The aim of this review is to provide a brief introduction to the principles of solid-state NMR spectroscopy and to highlight emerging trends which may further enhance the bioanalytical potential of solid-state NMR spectroscopy.

Solid-state NMR—a short introduction

The first successful NMR experiments on condensed matter were performed in 1945 [27, 28]. The famous Pake doublet in solids, i.e., the line shape resulting from the magnetic dipole–dipole interaction within isolated spin pairs, was

Published in the special issue on *Focus on Bioanalysis* with Guest Editors Antje J. Baeumner, Günter Gauglitz, and Frieder W. Scheller.

S. Paasch · E. Brunner (✉)
Fachrichtung Chemie und Lebensmittelchemie,
Bioanalytische Chemie, TU Dresden,
01062 Dresden, Germany
e-mail: eike.brunner@tu-dresden.de

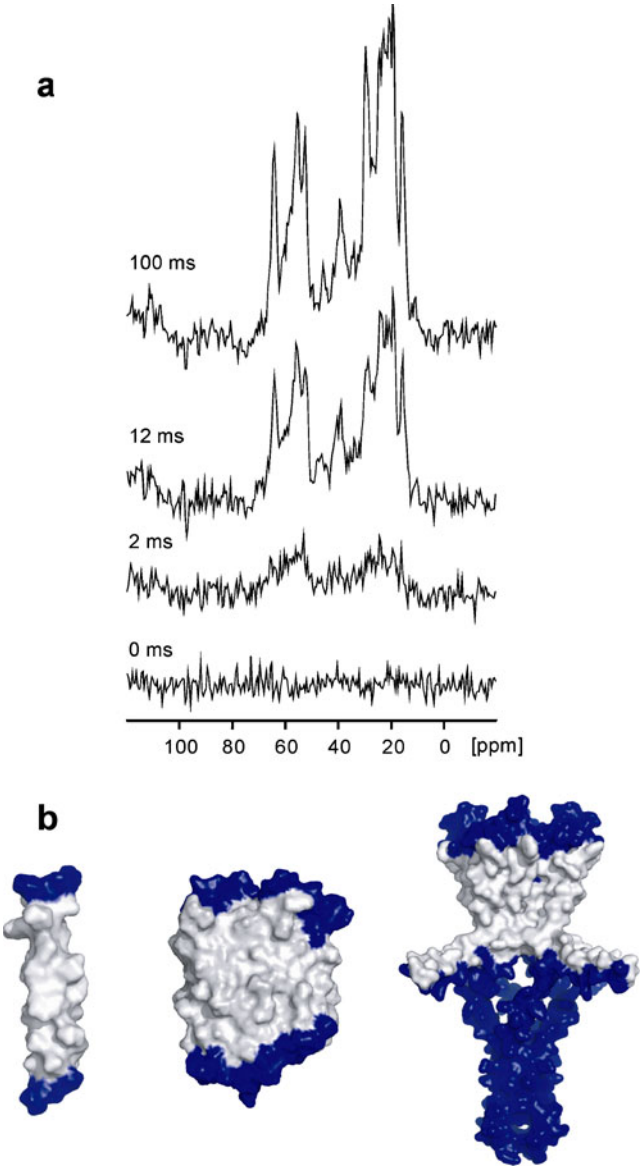

Fig. 1 Determination of water-accessible surfaces of membrane proteins in a lipid environment by 1D water-edited solid-state NMR spectroscopy. **a** ^{13}C-detected 1D water-edited cross-polarization (CP) experiments [15] performed on the chimeric ion channel KcsA-Kv1.3 at pH 7.5 with different longitudinal proton–proton mixing times as indicated. **b** Surface representations of three different membrane proteins studied by this experiment. From *left to right*, a monomeric phospholamban mutant (AFA-PLN), sensory rhodopsin from *Natronomonas pharaonis* (NpSRII), and the chimeric ion channel KcsA-Kv1.3. Water-accessible residues are labeled in *blue*. (Reproduced from Ader et al. [15] with permission from the American Chemical Society)

discovered in 1948 for the ^{1}H NMR signal of water molecules in hydrated crystals such as gypsum [29]. Apart from the homonuclear and heteronuclear magnetic dipole–dipole interactions between neighboring nuclei, the chemical shift anisotropy and—for nuclei with $I>1/2$—the electric quadrupole interaction are the dominating line-broadening interactions in solids [30]. The measurement of chemical shifts in solids, therefore, mandatorily requires the application of line-narrowing techniques to suppress the aforementioned line-broadening interactions as much as possible. This can be accomplished by mechanical spinning of the sample [31] around an axis tilted by the magic angle $\vartheta_m=54.7°$ with respect to the external magnetic field, $\boldsymbol{B}_0$, a technique which is denoted magic-angle spinning (MAS) or magic-angle sample spinning. Another approach for the suppression of homonuclear magnetic dipole–dipole interactions (homonuclear decoupling) is based on the irradiation of special pulse sequences [32, 33] such as the Waugh–Huber–Haeberlen (WAHUHA) sequence. Combined with MAS, combined rotation and multiple-pulse spectroscopy (CRAMPS) experiments result in an excellent spectral resolution for strongly coupled homonuclear spin systems such as ^{1}H and ^{19}F even if the available sample spinning rates are rather low (see Fig. 3) [33–35]. Especially in multidimensional NMR experiments, frequency-switched Lee–Goldburg (FSLG) or phase-modulated Lee–Goldburg (PMLG) decoupling or decoupling using mind-boggling optimization (DUMBO) is nowadays usually applied for homonuclear decoupling [36–38]. These sequences are designed such that the homonuclear magnetic dipole–dipole interaction is averaged out as efficiently as possible. The combination of MAS and multiple pulse sequences is necessary if the spin systems exhibit strong homogeneous interactions such as homonuclear magnetic dipole–dipole interactions among multiple spins. The suppression of these interactions would require extremely high sample spinning rates even beyond 100 kHz, which are not yet available (see later). However, the combination of MAS and the described pulse sequences results in superior resolution, as is shown in Fig. 3.

Solid-state NMR measurements of nuclei S with low gyromagnetic ratio γ_S such as ^{13}C, ^{15} N, and ^{29}Si using direct excitation are often extremely time-consuming (if not impossible). Their intrinsically low sensitivity is caused by the low spin polarization and sometimes low natural abundance in combination with rather long longitudinal relaxation times T_1 determining the repetition time between two subsequent scans (see later). Therefore, solid-state NMR spectra of the aforementioned nuclei are commonly acquired by cross-polarization (CP) experiments [39, 40]. The CP experiment is a typical polarization transfer experiment. Nuclei I of high magnetogyric ratio γ_I such as ^{1}H and ^{19}F typically serve as the source of magnetization, which is transferred to neighboring nuclei S. The physical basis of this polarization transfer is the heteronuclear magnetic dipole–dipole interaction between I and S. This experiment can result in a maximum signal enhancement given by γ_I/γ_S. For a ^{13}C{^{1}H} CP experiment (S is

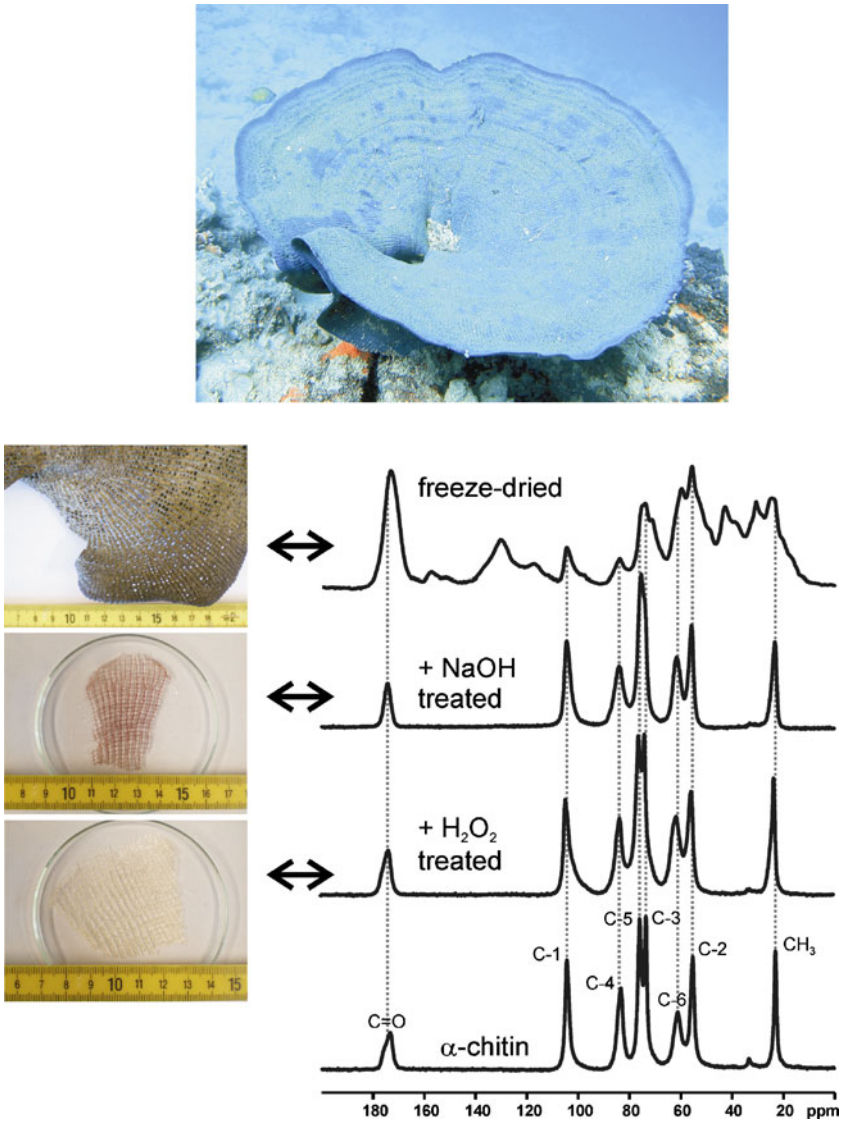

Fig. 2 An example for 1D solid-state ^{13}C NMR spectroscopy in bioanalytics. *Top*: Underwater photograph of a living marine demosponge, *Ianthella basta*. The diameter of the sponge corresponds to about 1 m. *Bottom*: Photographs of *I. basta* skeleton samples after different isolation steps and corresponding ^{13}C {^{1}H} CP magic-angle-spinning (MAS) NMR spectra. The spectrum of a reference α-chitin sample is shown for comparison. *Dashed vertical lines* indicate the chemical shifts of the signals in α-chitin. (Reproduced from [25] with permission from Elsevier)

^{13}C and I is ^{1}H), this maximum enhancement factor amounts to approximately 4. Since ^{1}H nuclei often exhibit a relatively short T_1 compared with the S nuclei, the effective signal-to-noise improvement factor within a given measurement time is usually much larger than γ_I/γ_S (see later). Ramped or adiabatic-passage CP experiments are nowadays often preferred [41–43]. Heteronuclear ^{1}H decoupling sequences such as two-pulse phase-modulated (TPPM) and small-phase incremental alternation (SPINAL) decoupling [44, 45] are commonly applied during signal acquisition to suppress the influence of the strongly coupled ^{1}H nuclei upon the line width of the S signals (^{13}C, ^{15}N, ^{29}Si, ^{31}P, etc.). Figure 4 demonstrates the application of the described techniques for the measurement of highly resolved solid-state ^{31}P NMR spectra of crystalline *O*-phospho-l-tyrosine. Note the shape of the ^{1}H-decoupled ^{31}P NMR signal measured without MAS which is mainly determined by the chemical shift anisotropy.

Fast MAS results in the removal of the influence of line-broadening interactions from the spectra. Especially the distance-dependent dipolar couplings are, however, a valuable source of structural information. Reintroduction of dipolar couplings allows the determination of internuclear distances. One frequently used technique is the rotational echo double resonance (REDOR) experiment [47] to selectively determine heteronuclear dipolar couplings. Rotational resonance experiments [48] allow the reintroduction of homonuclear dipolar couplings.

The application of multidimensional liquid-state NMR techniques [49] to proteins and other biomolecules in solution was a major breakthrough in biological NMR spectroscopy [1]. Multidimensional NMR spectroscopic techniques are also routinely used in solid-state NMR spectroscopy. Figure 5 shows a ^{1}H-^{31}P heteronuclear correlation (HETCOR) spectrum of the crystalline amino acid *O*-phospho-l-serine without and with homonuclear

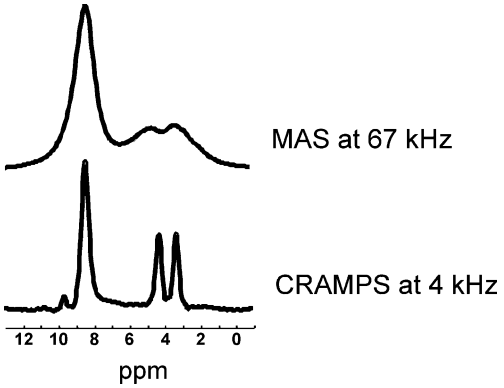

Fig. 3 Resolution in solid-state ^{1}H NMR spectroscopy: MAS versus combined rotation and multiple-pulse spectroscopy (*CRAMPS*). Note the remarkable improvement in resolution observed in the CRAMPS spectrum of crystalline glycine measured at only 4-kHz sample spinning rate compared with fast MAS at 67 kHz. (The spectra were kindly provided by U. Scheler, Leibniz Institute for Polymer Research Dresden)

FSLG decoupling during the evolution time t_1. The spectra were measured under MAS at a sample spinning rate ν_r of 12 kHz. Ramped ^{1}H-^{31}P CP was used for polarization transfer. Note the considerable improvement of resolution in the indirect spectral dimension (^{1}H spectrum) obtained by the application of homonuclear FSLG decoupling during the evolution time. The pulse scheme used for the FSLG decoupled experiment is given at top of the figure. This type of spectroscopy allows the detection of through-space correlations, dipolar couplings between different nuclei (here ^{1}H and ^{31}P). Through-bond correlations, i.e., *J* couplings, can be detected by a solid-state NMR experiment such as the incredible natural abundance double quantum transfer experiment (INADEQUATE) [50–52]) or total through-bond correlation spectroscopy (TOBSY) [53]. Furthermore, insensitive nuclei enhanced by polarization transfer (INEPT) experiments—originally designed for heteronuclear liquid-state NMR spectroscopy [2]—are also feasible in solid-state NMR spectroscopy [54], especially under efficient homonuclear ^{1}H decoupling and at high sample spinning rates for biological samples [55, 56].

In addition to the structural information described, solid-state NMR spectroscopy also allows the determination of dynamics such as intramolecular motions within the biomolecules. One possibility is the analysis of relaxation data, i.e., the study of the influence of thermal motions

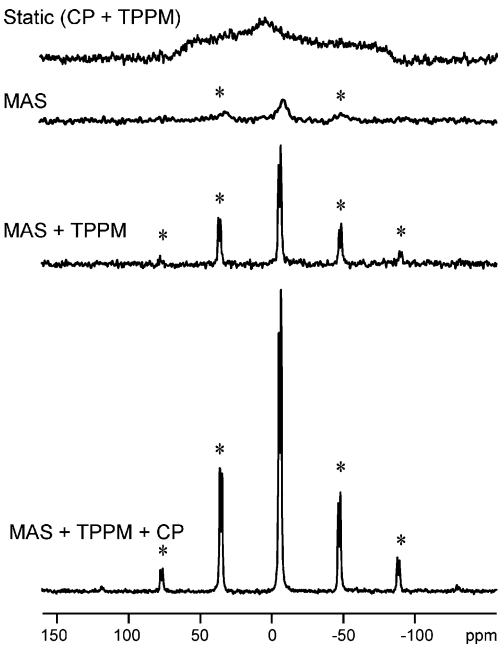

Fig. 4 Demonstration of typical solid-state NMR techniques. Experimental solid-state ^{31}P NMR spectra of *O*-phospho-l-tyrosine measured at B_0=7.05 T (T=302 K). From *top to bottom*, static spectrum measured using CP and heteronuclear two-pulse phase-modulated (*TPPM*) decoupling, MAS NMR spectrum acquired without CP and heteronuclear decoupling, MAS NMR spectrum measured without CP but under heteronuclear TPPM decoupling, and MAS NMR spectrum acquired with CP and heteronuclear TPPM decoupling (ν_r=5 kHz, 16 scans). *Asterisks* denote spinning sidebands. (Reproduced from [46] with permission from Elsevier)

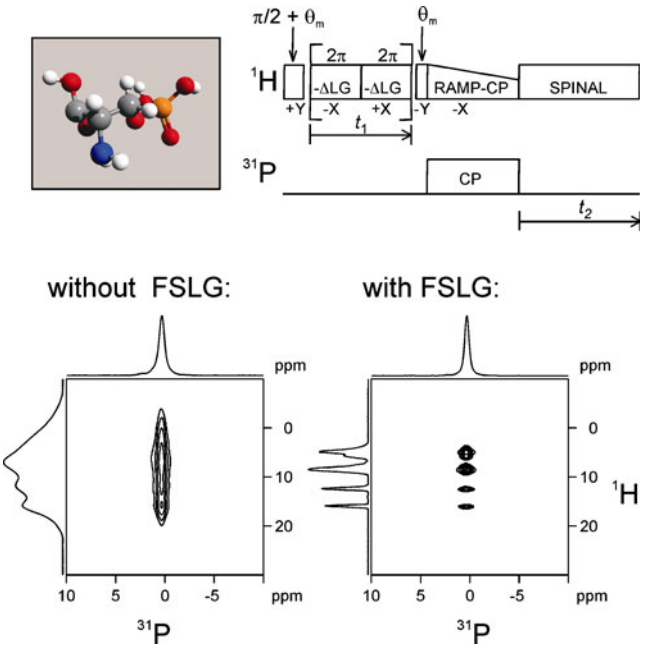

Fig. 5 2D correlation spectroscopy. ^{1}H-^{31}P heteronuclear correlation (HETCOR) spectrum of crystalline *O*-phospho-l-serine measured at room temperature and a sample spinning rate of 12 kHz using small-phase incremental alternation (*SPINAL*) ^{1}H decoupling during signal acquisition. Ramped CP with a mixing time of 2 ms was applied. The spectrum was measured without (*bottom left*) and with (*bottom right*) frequency-switched Lee–Goldburg (*FSLG*) decoupling during the evolution time. Note the remarkable resolution improvement in the ^{1}H dimension resulting from this homonuclear decoupling technique. A structural model of *O*-phospho-l-serine as well as the pulse scheme employed for the FSLG decoupled spectrum are shown at the *top*

upon the longitudinal and transverse relaxation times T_1 and T_2, respectively. This could recently be applied to investigate the mobility of chondroitin sulfate in articular and artificial cartilage [57]. It should be noted that the presence of thermal motions influences the shape and line width of MAS NMR signals in a characteristic manner depending on the correlation time, τ_C, of the motional processes (see "Spectral resolution"). Elaborate techniques have been developed for the study of proteins: For example, mobile protein segments can be detected using the through-bond correlation schemes introduced by Andronesi et al. [5]. Conformational dynamics in proteins with correlation times between milliseconds and seconds become detectable in dipolar centerband-only detection of exchange (CODEX) NMR experiments [58, 59] (see Fig. 6).

Sensitivity and spectral resolution are the crucial parameters which determine and limit the applicability of any spectroscopic technique. Often, the available amounts of biological samples are rather limited—in particular if isotope labeling is necessary. The detection of very small amounts of sample is, therefore, particularly important for bioanalytical applications. Furthermore, the complex biomolecules often exhibit numerous signals, resulting in resolution problems. The following sections are, therefore, devoted to the discussion of sensitivity and resolution especially with respect to novel biological applications of solid-state NMR spectroscopy.

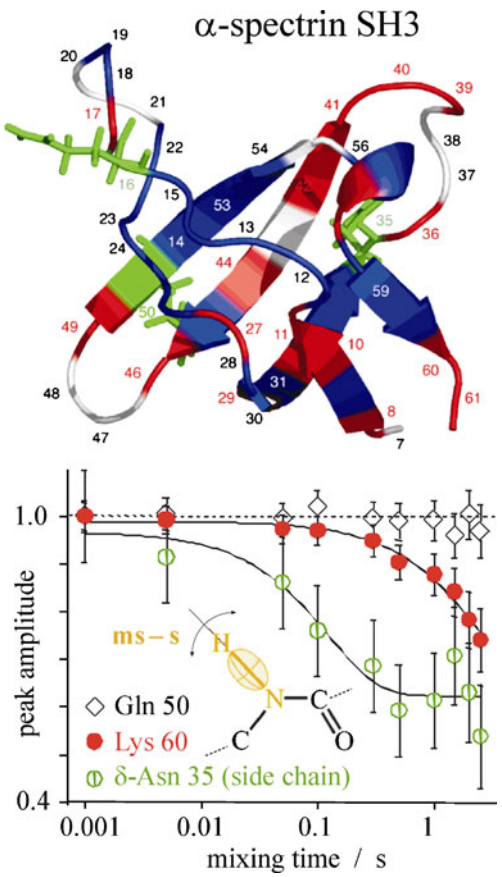

Fig. 6 Detection of slow conformational dynamics by dipolar centerband-only detection of exchange (CODEX). *Top*: Structure of the α-spectrin SH_3 domain with colour-coded residue mobility. *Blue* indicates immobile residues and *red* (backbone) and *green* (side chains) indicate mobile residues. Unassigned or undetected residues are shown in *white*. (Reproduced from Krushelnitsky et al. [58] with permission from the American Chemical Society)

Improvements in sensitivity

The signal-to-noise ratio obtained in an NMR experiment depends on the macroscopic magnetization of the sample, which is determined by the spin polarization *P*. The spin polarization is given by

$$P = 100\% \frac{|N_{+1/2} - N_{-1/2}|}{N_{+1/2} + N_{-1/2}} \quad (1)$$

for spin-1/2 nuclei. Here, $N_{+1/2}$ and $N_{-1/2}$ are the populations of the two Zeeman energy levels corresponding to magnetic spin quantum numbers +1/2 and -1/2, respectively. These populations are given by the Boltzmann distribution in thermal equilibrium. For spin-1/2 nuclei, one can write within the high-temperature approximation, which is valid at room temperature and the currently available magnetic fields,

$$P = 100\% \frac{\hbar \gamma_I B_0}{2kT}. \quad (2)$$

$\hbar$ is the Planck constant divided by 2π, k denotes the Boltzmann constant, and T is the absolute temperature. Note that the signal-to-noise ratio also depends on various other parameters, for example, the coil filling factor, the sample volume, the noise figure of the preamplifier, and the temperature of the detection coil [60, 61]. Furthermore, the signal-to-noise ratio increases with the square root of the number of scans which are added to acquire the free-induction decay. The repetition time between two subsequent scans is limited by the longitudinal relaxation time. After a $\pi/2$ excitation pulse, polarization buildup times of about 5 times T_1 are commonly allowed before the next scan. Consequently, the signal-to-noise ratio depends on the square root of the measurement time.

As can be seen from Eq. 2, the spin polarization and hence the signal-to-noise ratio can be enhanced by increasing the magnetic field $\boldsymbol{B}_0$. Over the past few decades, the field strength of commercial spectrometers has continuously increased. Nowadays, superconducting magnets up to approximately 23 T are available. Pulsed magnets with maximum fields up to 56 T could be developed and used for the detection of ^{1}H NMR spectra

[62]. However, the room-temperature equilibrium spin polarization P of ^{1}H nuclei amounts to only 0.02% even at 56 T. This is the physical reason for the intrinsically low sensitivity of NMR spectroscopy. Therefore, sensitivity improvement remains one of the major methodical challenges in NMR spectroscopy [63, 64].

The spin polarization can be enhanced by sample cooling in special cases. This, however, requires very low temperatures, which cannot always be applied, especially in the case of biological samples. Furthermore, MAS at temperatures below approximately 100 K is technically difficult. The creation of nonequilibrium spin polarizations by hyperpolarization experiments is, therefore, an important field of methodical development.

Hyperpolarization methods

We have already described the advantages of the CP experiment. However, the maximum polarization gain in this experiment is limited by γ_I/γ_S. Other techniques are capable of delivering considerably higher spin polarizations. Promising hyperpolarization approaches which have already been exploited for solids or solid surfaces are dynamic nuclear polarization (DNP), chemically induced nuclear polarization (CIDNP)/photochemically induced nuclear polarization (photo-CIDNP), and spin-exchange optical pumping (SEOP).

DNP relies on the spin-polarization transfer from electrons to nuclei [65] (see also Fig. 7). In the case of diamagnetic samples, the samples have to be doped with appropriate paramagnetic agents [66]. The paramagnetic substances can be brought into contact with the molecules of interest, for example, by freezing glass-forming solutions containing paramagnetic solutes as well as the sample molecules. Spin diffusion among ^{1}H nuclei can result in the efficient distribution of the DNP-enhanced nuclear spin polarization throughout the samples. The past few years have seen considerable methodical progress in DNP experiments [67–69] which made it possible to combine DNP with MAS. These methodical advances are currently paving the way to a variety of novel bioanalytical applications [70–72].

The CIDNP effect was discovered in 1967 independently by two groups [73–75]. It occurs as a result of radical ion reactions and is often explained by the radical pair mechanism. The electron-spin-dependent recombination probability of radical pairs is influenced by the nuclear spin, i.e., the hyperfine coupling between electrons and nuclear spins. Therefore, reactions involving radical pairs can result in strongly enhanced nuclear spin polarizations; for details, see the recent review by Bargon [76]. Photo-CIDNP was discovered shortly after the first CIDNP experiments had been performed [77, 78]. Since then,

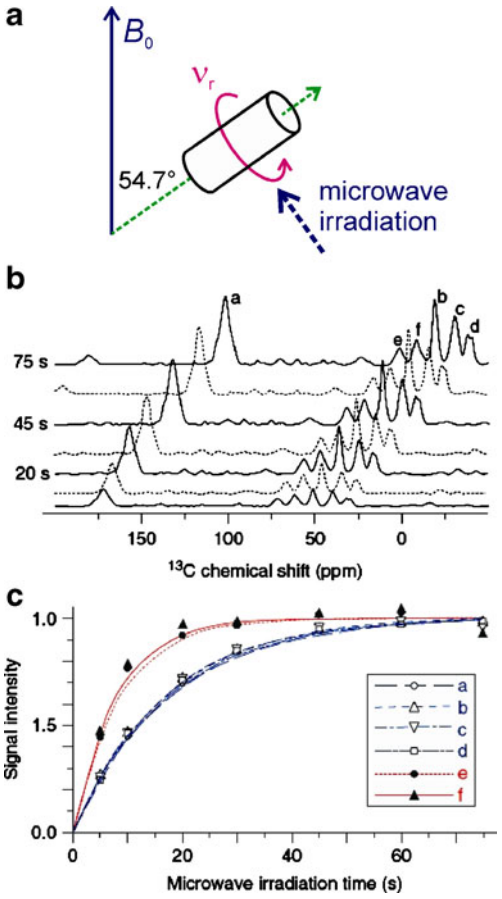

Fig. 7 Dynamic nuclear polarization (DNP). **a** The solid-state DNP experiment under MAS. **b** Time-dependent growth of 1D ^{13}C NMR signals of a nanocrystalline, amyloidogenic peptide (GNNQQNY$_{7\text{-}13}$) using a biradical polarizing agent (TOTAPOL). The spectra were acquired after 5, 10, 20, 30, 45, 60, and 75 ms of microwave irradiation. **c** The intensity of the spectral lines normalized to maximum intensity of each signal. *Lines* indicate calculated fits using growth time constants of 15–17 s for crystal signals (*a*–*d*) and 7–8 s for glycerol peaks (*e*, *f*). The samples were prepared by mixing peptide nanocrystals with glycerol containing the biradical TOTAPOL as described in [70]. (**a**, **b** Reproduced from van der Wel et al. [70] with kind permission from the American Chemical Society)

photo-CIDNP has become an important tool for photobiochemical investigations. Photo-CIDNP could also be combined with MAS [79] to study photobiochemical processes by solid-state NMR spectroscopic techniques [80–83].

SEOP is an experimental approach which can be applied to hyperpolarize noble gases such as ^{129}Xe (see Fig. 8 as well as [84–86]). Optical pumping of alkali atoms, usually Rb, results in highly polarized electron spin systems. Electron spin polarization is then transferred to the nuclear spins by the formation of short-lived Rb–Xe van der Waals complexes or Rb–Xe collisions via hyperfine coupling. These processes lead to a ^{129}Xe spin polarization 4 to 5 orders of magnitude higher than the equilibrium spin polarization in commonly used spectrometers. ^{129}Xe is an

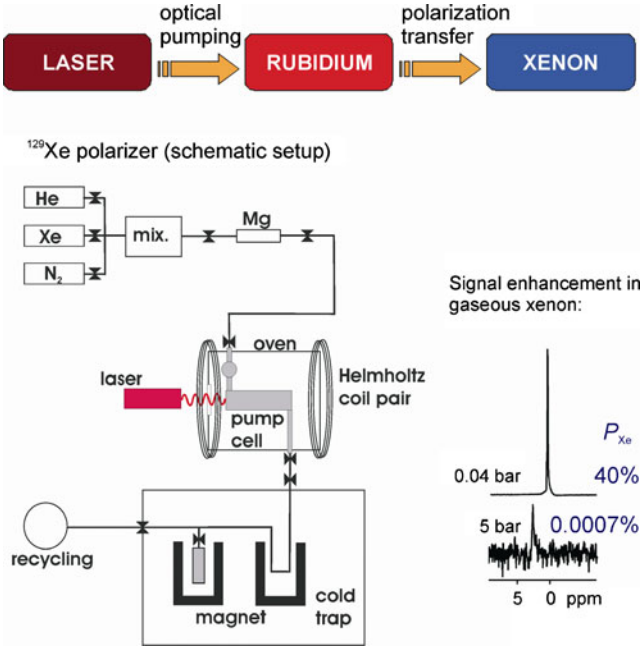

Fig. 8 Spin-exchange optical pumping (SEOP). *Top*: The SEOP process. *Bottom left*: The setup of a typical xenon polarizer. *Bottom right*: Demonstration of the sensitivity gain obtained for the ^{129}Xe NMR signal of xenon gas. The bottom spectrum was measured in thermal equilibrium at 5 bar, $\boldsymbol{B}_0$=7.04 T. The top spectrum was obtained for hyperpolarized ^{129}Xe at 0.04 bar (40% spin polarization). (The graphic at the *bottom left* is reproduced from Fink et al. [86] with permission from the American Physical Society)

important probe atom which was originally introduced by Ito and Fraissard [87] in surface NMR spectroscopy. Hyperpolarized xenon was then suggested to enhance the NMR of solid surfaces [88]. In addition, xenon is also frequently used in biological NMR spectroscopy [89–97] as well as for imaging purposes [98, 99]. SEOP, therefore, offers a variety of solid- and liquid-state NMR experiments (for reviews, see [96, 97]) even under MAS [100], including spin-polarization-transfer techniques such as the spin-polarization-induced nuclear Overhauser effect (SPINOE) [101] and spin-polarization-induced enhancement by Hartmann–Hahn dipolar recoupling (SPIDER) [102]. Biosensor applications of xenon have recently found special interest in biological liquid-state NMR spectroscopy as well as in imaging [103–105].

Enhanced spin polarizations can also be produced by hydrogenation reactions using parahydrogen [106, 107]. This parahydrogen-induced polarization (PHIP) effect can be created either in high field (parahydrogen and synthesis allow dramatically enhanced nuclear alignment, PASADENA [106]) or in low field (adiabatic longitudinal transport after dissociation engenders net alignment, ALTADENA [108]). PHIP is increasingly being exploited in liquid-state NMR spectroscopy [109], for example, in spin-polarization-transfer experiments [110, 111]. The PASADENA approach could be applied to study H_2 chemisorption on ZnO [112]. Recently, Adams et al. [113] developed an approach for the reversible interaction of parahydrogen with organic substrates mediated by metal complexes. This approach results in signal enhancement factors up to approximately 800 in ^{1}H, ^{13}C, and ^{15}N NMR and can be used in magnetic resonance imaging as well. Finally, it should be mentioned that hyperpolarized spin systems provide the basis for extremely fast 2D experiments, so-called ultrafast 2D NMR spectroscopy [114]. In contrast to conventional 2D NMR spectroscopy, such techniques allow the detection of 2D spectra within a single scan or only a few scans.

T_1 shortening and related approaches

As already mentioned, the signal-to-noise ratio obtained in an experiment after a certain time increases strongly if T_1 is short. T_1 shortening is, therefore, another promising approach for sensitivity enhancement. The addition of Cu(II)Na_2EDTA as a chelated paramagnetic relaxation agent results in about 2 orders of magnitude shorter T_1 values for protein microcrystals [115]. Linser et al. [116] combined this approach with partial deuteration of the samples by the recrystallization of a protein in 9:1 D_2O/H_2O solution in the presence of the relaxation agent. Paramagnetic doping of solid proteins such as amyloid fibers and ubiquitin was combined with very fast MAS and low-power radio-frequency pulse sequences in the paramagnetic-relaxation-assisted condensed data collection (PACC) experiment [117]. This experiment results in a reduction of T_1 by orders of magnitude and allows the detection of 2D solid-state NMR spectra for protein concentrations in the nanomolar range.

Another time-saving solid-state NMR approach is the relaxation enhancement by a lower temperature of adjacent spins (RELOAD) experiment [118]. This experiment is based on the idea that selective excitation of spins such as ^{13}C which are strongly coupled to ^{1}H nuclei is followed by enhanced relaxation due to ^{1}H-driven spin diffusion from nonexcited spins, thus resulting in faster magnetization recovery.

Microcoils

The sensitivity of an NMR experiment on a sample of given volume depends on the coil filling factor, i.e., the ratio between the coil volume and the sample volume. If the available sample volume is rather small, the use of microcoils results in a significant improvement in the signal-to-noise ratio. The need to study low sample volumes especially in biological NMR spectroscopy has stimulated numerous attempts to develop appropriate

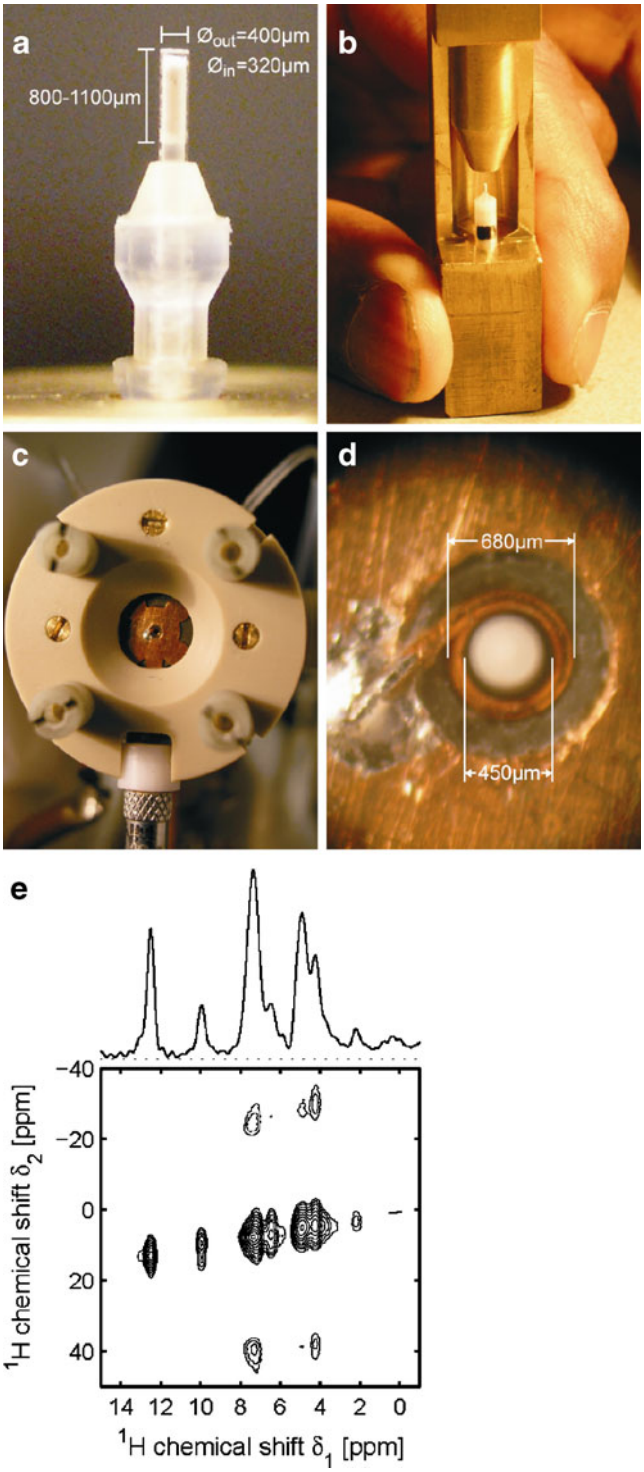

Fig. 9 Microcoil MAS probehead for ^{1}H spectroscopy [122]. **a** Kel-F holder with inserted fused-silica capillary containing powdered sample material. The capillary has inner and outer diameters of 320 and 400 µm, respectively. The sample height is 800–1,100 µm, leaving some space to close off the capillary with Teflon tape. Typical sample volumes of 64–88 nl result. **b** A 2.5-mm Varian rotor with a Kel-F holder and capillary inside the custom-made press-on tool. **c** Upper front of the 2.5-mm Varian stator with the mounted holder of the solenoid microcoil. **d** Microscope image of the silica capillary spinning inside the microcoil. The radio-frequency coil has 7.5 windings and the isolated copper wire has a diameter of 115 µm. The inner and outer diameters of the radio-frequency coil are 450 and 680 µm, respectively. **e** 2D ^{1}H spectrum of a single crystal of l-tyrosine–HCl with dimensions 230×230×800 µm^3=42 nl obtained at 9.4 T and 12-kHz MAS frequency, where FSLG homonuclear decoupling was applied in the indirect ^{1}H dimension. (Reproduced from Brinkmann et al. [122] with permission from Elsevier)

microcoil systems also for solid-state NMR spectroscopy [119–124]. Solenoid microcoil systems have been developed for wide-line solid-state NMR spectroscopy [119]. In addition, even MAS NMR spectroscopy of nanoliter samples became feasible: one approach uses a conventional rotor as a carrier of a capillary containing the nanoliter-sized sample (see Fig. 9) [121–123]. Despite this extremely small sample volume, the sensitivity is even sufficient for 2D experiments [122] as well as quadrupolar tensor determination [123]. Another approach is the magic-angle coil spinning (MACS) experiment [124]. A tuned microcoil is tightly wound around the sample, which is placed in a glass capillary. The capillary and the microcoil are then inserted into a conventional MAS rotor. Wireless coupling between the tuned microcoil and the probe generates a high radio-frequency field and leads to enhanced detection sensitivity.

Spectral resolution

As already stated, solid-state NMR spectroscopy usually relies on the application of line-narrowing techniques, in particular MAS. The spectral resolution is, therefore, determined by the residual line width of the MAS-narrowed signals. Apart from trivial experimental imperfections such as a misadjustment of the magic angle, field inhomogeneities, etc., the residual line width of MAS NMR signals is determined by the following effects [125–131]:

1. The incomplete suppression of the line-broadening influence of internal magnetic interactions. This is particularly true for the influence of strong homonuclear dipolar couplings (e.g., among ^{1}H or ^{19}F nuclei) as well as second-order quadrupolar effects for $I>1/2$.
2. The interfering effect of random molecular motions with the coherent averaging techniques of MAS and heteronuclear decoupling [129–131]. This effect is demonstrated in Fig. 10.
3. Distributions of the isotropic chemical shift which may be caused by distributions of parameters such as bond lengths, bond angles, etc.
4. Distribution of the isotropic value of the magnetic susceptibility and line-broadening due to the anisotropy of the magnetic susceptibility.

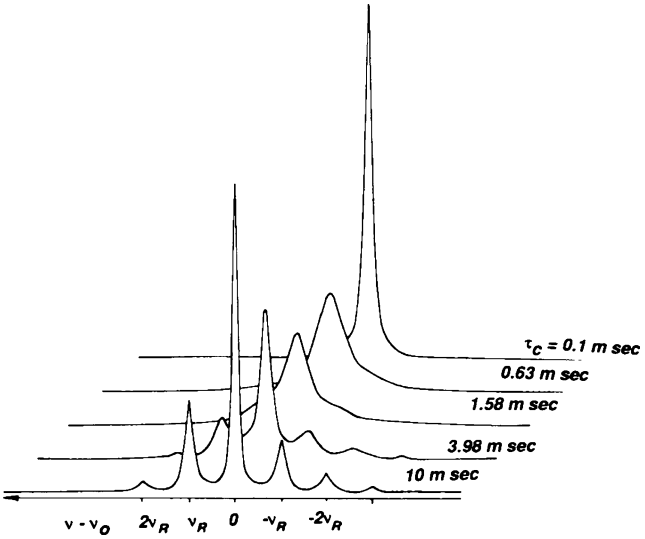

Fig. 10 The influence of thermal motions upon MAS NMR signals. MAS NMR spectra for dominating chemical shift anisotropy (CSA) were calculated as a function of the correlation time τ_C of the thermal motions. Sample spinning rate 1 kHz, $\omega_I\beta_{CSA}$ 2 kHz, η_{CSA} 0.5. Increasingly fast motions (i.e., decreasing correlation times τ_C) are accompanied by an increasingly strong line broadening and gradually disappearing spinning sidebands. The maximum residual line width, i.e., worst spectral resolution, is obtained for $\nu_r=1/\tau_C$. For further decreasing correlation times, the signals become narrower owing to motional averaging similar to the behavior observed in liquid-state NMR spectroscopy. (Reproduced from [131] with permission from Academic Press)

In particular the effects described in item 1 are strongly influenced by the external magnetic field $\boldsymbol{B}_0$ as well as the sample spinning rate ν_r. To evaluate the influence of $\boldsymbol{B}_0$ and ν_r on the spectral resolution, it should be remembered that the frequency difference between two neighboring signals of given chemical shift difference $\Delta\delta$ increases linearly. That means the resolution increases linearly if the residual line width of the two signals remains constant at the frequency scale, i.e., if the magnetic interactions responsible for the residual line width do not depend on $\boldsymbol{B}_0$. This is, in principle, true for the magnetic dipole–dipole interaction. Strong homonuclear magnetic dipole–dipole interactions among *magnetically equivalent* nuclei can only be averaged out completely by very high sample spinning rates [126–128] or in CRAMPS experiments (see earlier). The residual line width of spin systems such as ^{1}H is dominated by the homonuclear magnetic dipole–dipole interaction and can be written as follows:

$$\Delta\nu_{1/2}^{MAS} = \frac{1}{A}\frac{(\Delta\nu_{II})^2}{\nu_r}. \quad (3)$$

$\Delta\nu_{II}$ denotes the homonuclear contribution to the static line width, i.e., the line width without MAS. The geometry-dependent factor A is typically found within the range 10–40 [126]. That means the residual line width is proportional to $1/\nu_r$ (see also Fig. 11) and the suppression of the homonuclear magnetic dipole–dipole interaction would require sample spinning far beyond 100 kHz [126, 127], which is not yet possible. This is the reason why directly detected ^{1}H MAS NMR spectra of such systems are often poorly resolved. It is, however, important to note that the spectral resolution in homonuclear spin systems may increase even more strongly than linear in $\boldsymbol{B}_0$. The reason for this unexpected behavior is the truncation of the Hamiltonian in homonuclear spin systems at high fields resulting in a reduction of the line width with increasing $\boldsymbol{B}_0$ even at the frequency scale [132].

The past decade also saw considerable progress in the development of faster MAS probes [128]. Maximum sample spinning rates of approximately 70 kHz are now available. Combined with suitable homonuclear decoupling techniques [133, 134], such high sample spinning rates result in solid-state ^{1}H NMR spectra of considerable spectral resolution.

Another possibility to reduce the homonuclear magnetic dipole–dipole interaction in strongly coupled ^{1}H spin systems such as solid proteins is partial deuteration, a method which allows the measurement of highly resolved ^{1}H-detected spectra of proteins in the solid state. This is of special interest: Multidimensional solid-state NMR spectra of proteins are usually not ^{1}H-detected owing to the rather poor spectral resolution. For sensitivity reasons, however, ^{1}H detection is highly desirable (see earlier) and, hence, commonly applied in multidimensional liquid-state NMR spectroscopy of proteins. At high levels of deuteration, extremely well resolved solid-state ^{1}H NMR spectra of proteins can be detected [135]. The optimum exchange level of exchangeable protons in solid proteins amounts to

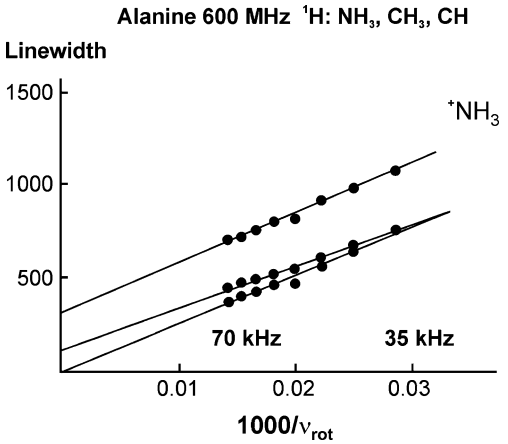

Fig. 11 Residual line width (Hz) of the ^{1}H MAS NMR signals of alanine as a function of $1/\nu_r$ measured at 600 MHz. The available sample spinning rates do not result in a complete removal of the influence of the homonuclear magnetic dipole–dipole interaction. (Reproduced from Samoson et al. [128] with permission from Springer)

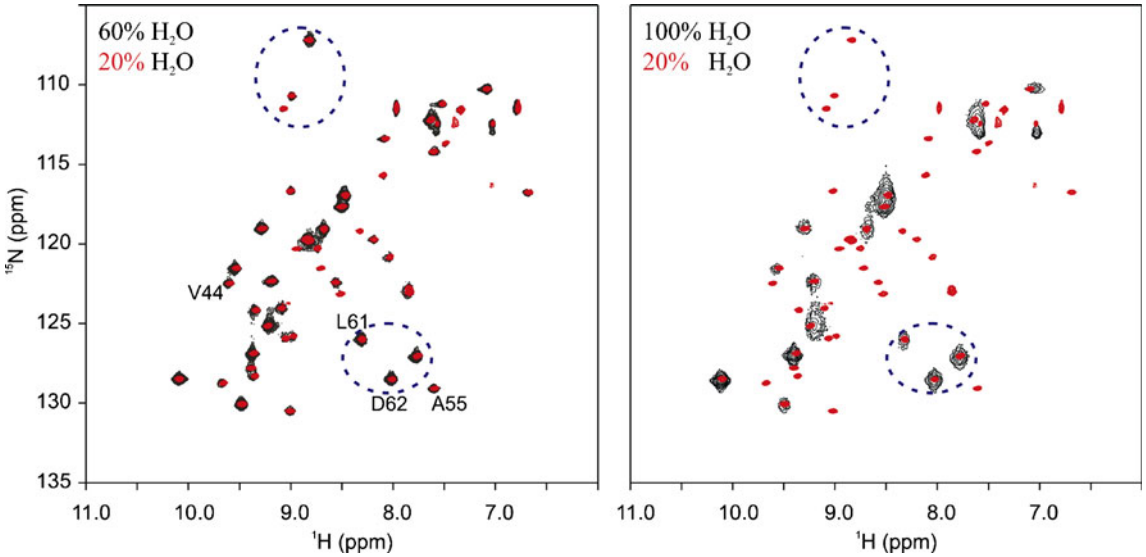

Fig. 12 ^{1}H-detected ^{1}H-^{15} N HETCOR spectra of the α-spectrin SH_3 domain for samples recrystallized in H_2O/D_2O solutions containing 20, 60, and 100% H_2O in the crystallization buffer. The spectrum recorded for the sample prepared with 20% exchangeable protons is shown in *red*. Two classes of cross-peaks are highlighted belonging to residues which are either remaining or disappearing in the spectra in the sample prepared with 100% H_2O in the crystallization buffer. (Reproduced from Akbey et al. [136] with permission from Springer)

30–40%, as could be measured recently [136] (see also Fig. 12). HETCOR experiments on crystalline, perdeuterated proteins allow the identification of hydroxyl protons, the study of their hydrogen bonds, and determination of exchange dynamics [137].

The line width and shape of nuclei with $I>1/2$ is usually determined by the electric quadrupole interaction in second-order perturbation theory [138]. This broadening is proportional to $1/\boldsymbol{B}_0$; therefore, increasing field strengths lead to a corresponding nonlinear improvement of spectral resolution.

Finally, it should be noted that the line width increases linearly with $\boldsymbol{B}_0$ at the frequency scale if the residual line width reaches the limiting "natural" line width determined by the distribution of the isotropic chemical shift and/or the magnetic susceptibility of the sample. Increasing magnetic fields do then not further improve spectral resolution.

Conclusions

Triggered by continuous methodical advances, solid-state NMR spectroscopy is increasingly important for the study of biological problems. Apart from stronger magnetic fields and faster MAS devices, remarkable methodical improvements are, for example:

- Hyperpolarization techniques (DNP, CIDNP/photo-CIDNP, SEOP)
- Microcoils in combination with MAS (nanoliter samples!)
- T_1 shortening for sensitivity improvement.

Prominent biological applications of solid-state NMR spectroscopy are:

- Membrane proteins/peptides
- Protein aggregates such as amyloid fibrils
- Photobiochemical processes (e.g., by photo-CIDNP experiments)
- Investigations of integer cells
- Biomineralization phenomena

Solid-state NMR spectroscopy can serve as an analytical tool to identify substances by characteristic spectroscopic parameters (chemical shifts, *J*-coupling constants, etc.). Furthermore, solid-state NMR spectroscopy allows investigations of the spatial structure as well as dynamics of biomolecules without the need for crystalline samples. The capability of characterizing dynamical processes is the reason why solid-state NMR spectroscopy is often useful even for crystalline samples because the provided information complements the structural information obtained by diffraction studies. In summary, it can be stated that solid-state NMR spectroscopy is an increasingly important tool in bioanalytics.

Acknowledgements The authors wish to thank Annett Bachmann and Renate Schulze for carefully proofreading the manuscript. Financial support from the Deutsche Forschungsgemeinschaft (BR 1278/ 12) is gratefully acknowledged.

References

1. Wüthrich K (1986) NMR of proteins and nucleic acids. Wiley, New York
2. Cavanagh J, Fairbrother WJ, Palmer AG III, Skelton NJ (1996) Protein NMR spectroscopy, principles and practice. Academic, San Diego
3. Castellani F, van Rossum B, Diehl A, Schubert M, Rehbein K, Oschkinat H (2002) Nature 420:98
4. Baldus M (2007) J Biomol NMR 39:73
5. Andronesi OC, Becker S, Seidel K, Heise H, Young HS, Baldus M (2005) J Am Chem Soc 127:12965
6. Tycko R (2006) Methods Enzymol 413:103
7. Müller SD, Angeliss AA, Walther TH, Grage SL, Lange C, Opella SJ, Ulrich AS (2007) Biochim Biophys Acta 1768:3071
8. Laage S, Marchetti A, Sein J, Pierattelli R, Sass HJ, Grzesiek S, Lesage A, Pintacuda G, Emsley L (2008) J Am Chem Soc 130:17216
9. Manolikas T, Herrmann T, Meier BH (2008) J Am Chem Soc 130:3959
10. Strandberg E, Kanithasen N, Tiltak D, Bürck J, Wadhwani P, Zwernemann O, Ulrich AS (2008) Biochemistry 47:2601
11. Wadhwani P, Bürck J, Strandberg E, Mink C, Afonin S, Ulrich AS (2008) J Am Chem Soc 130:16515
12. Aisenbrey C, Bechinger B, Gröbner G (2008) J Mol Biol 375:376
13. Ader C, Schneider R, Hornig S, Velisetty P, Wilson EM, Lange A, Giller K, Ohmert I, Martin-Eauclaire MF, Trauner D, Becker S, Pongs O, Baldus M (2008) Nat Struct Mol Biol 15:605
14. Park SH, Loudet C, Marassi FM, Dufourc EJ, Opella SJ (2008) J Magn Reson 193:133
15. Ader C, Schneider R, Seidel K, Etzkorn M, Becker S, Baldus M (2009) J Am Chem Soc 131:170
16. Ader C, Schneider R, Hornig S, Velisetty P, Vardanyan V, Giller K, Ohmert I, Becker S, Pongs O, Baldus M (2009) EMBO J 28:2825
17. Paravastu AK, Qahwash I, Leapman RD, Meredith SC, Tycko R (2009) Proc Natl Acad Sci USA 106:7443
18. McDermott A (2009) Annu Rev Biophys 38:385
19. Sani MA, Keech O, Gardeström P, Dufourc EJ, Gröbner G (2009) FASEB J 23:2872
20. Resende JM, Moraes CM, Munhoz VH, Aisenbrey C, Verly RM, Bertani P, Cesar A, Pilo-Veloso D, Bechinger B (2009) Proc Natl Acad Sci USA 106:16639
21. Aisenbrey C, Bertani P, Bechinger B (2010) Methods Mol Biol 618:209
22. Wu CH, Das BB, Opella SJ (2010) J Magn Reson 202:127
23. Gröger C, Lutz K, Brunner E (2009) Prog Nucl Magn Reson Spectrosc 54:54
24. Gröger C, Sumper M, Brunner E (2008) J Struct Biol 161:55
25. Brunner E, Ehrlich H, Schupp P, Hedrich R, Hunoldt S, Kammer M, Machill S, Paasch S, Bazhenov VV, Kurek D, Arnold T, Brockmann S, Ruhnow M, Born R (2009) J Struct Biol 168:539
26. Brunner E, Richthammer P, Ehrlich H, Paasch S, Simon P, Ueberlein S, van Pée K-H (2009) Angew Chem Int Ed 48:9724
27. Purcell EM, Torrey HC, Pound RV (1946) Phys Rev 69:37
28. Bloch F, Hansen WW, Packard M (1946) Phys Rev 70:474
29. Pake GE (1948) J Chem Phys 16:327
30. Mehring M (1983) Principles of high-resolution NMR in solids, 2nd edn. Springer, Berlin
31. Andrew ER, Bradbury A, Eades RG (1958) Nature 182:1659
32. Waugh JS, Huber LM, Haeberlen U (1968) Phys Rev Lett 20:180
33. Haeberlen U, Waugh JS (1968) Phys Rev 175:453
34. Pembleton RG, Ryan LM, Gerstein BC (1977) Rev Sci Instrum 48:1286
35. Scheler G, Haubenreisser U, Rosenberger H (1981) J Magn Reson 44:134
36. Bielecki A, Kolbert AC, Levitt MH (1989) Chem Phys Lett 155:341
37. Vinogradov E, Madhu PK, Vega S (1999) Chem Phys Lett 314:443
38. Sakellariou D, Lesage A, Hodgkinson P, Emsley L (2000) Chem Phys Lett 319:253
39. Pines A, Waugh JS, Gibby MG (1972) J Chem Phys 56:1776
40. Pines A, Gibby MG, Waugh JS (1973) J Chem Phys 59:569
41. Metz G, Wu X, Smith SO (1994) J Magn Reson A 110:219
42. Hediger S, Meier BH, Kurur ND, Bodenhausen G, Ernst RR (1994) Chem Phys Lett 223:283
43. Hediger S, Meier BH, Ernst RR (1995) Chem Phys Lett 240:449
44. Bennett AE, Rienstra CM, Auger M, Lakshmi KV, Griffin RG (1995) J Chem Phys 103:6951
45. Fung BM, Khitrin AK, Ermolaev K (2000) J Magn Reson 142:97
46. Iuga A, Ader C, Gröger C, Brunner E (2007) Annu Rep NMR Spectrosc 60:145
47. Gullion T, Schaefer J (1989) J Magn Reson 81:196
48. Levitt MMH, Raleigh DP, Creuzet F, Griffin RG (1990) J Chem Phys 92:6347
49. Ernst RR, Bodenhausen G, Wokaun A (1987) Principles of nuclear magnetic resonance in one and two dimensions. Clarendon Press, Oxford
50. Bax A, Freeman R, Kempsell SP (1980) J Am Chem Soc 102:4849
51. Levitt MH, Ernst RR (1983) Mol Phys 50:1109
52. Lesage A, Bardet M, Emsley L (1999) J Am Chem Soc 121:10987
53. Baldus M, Meier BH (1996) J Magn Reson A 121:65
54. Fyfe CA, Wong-Moon KC, Huang Y, Grondey H (1995) J Am Chem Soc 117:10397
55. Elena B, Lesage A, Steuernagel S, Böckmann A, Emsley L (2005) J Am Chem Soc 127:17296
56. Mao K, Pruski M (2009) J Magn Reson 201:165
57. Scheidt HA, Schibur S, Magalhães A, de Azevedo ER, Bonagamba TJ, Pascui O, Schulz R, Reichert D, Huster D (2010) Biopolymers 93:520
58. Krushelnitsky A, de Azevedo E, Linser R, Reif B, Saalwächter K, Reichert D (2009) J Am Chem Soc 131:12097
59. Li W, McDermott A (2009) J Biomol NMR 45:227
60. Abragam A (1961) Principles of nuclear magnetism. Oxford University Press, Oxford
61. Hoult DI, Richards RE (1976) J Magn Reson 24:71
62. Kozlov MB, Haase J, Baumann C, Webb AG (2005) Solid State Nucl Magn Reson 28:64
63. Spiess HW (2008) Angew Chem Int Ed 47:639
64. Opella SJ (2009) Nat Meth 6:197
65. Abragam A, Goldman M (1978) Rep Prog Phys 41:395
66. Matsuki Y, Maly T, Ouari O, Karoui H, Le Moigne F, Rizzato E, Lyubenova S, Herzfeld J, Prisner T, Tordo P, Griffin RG (2009) Angew Chem Int Ed 48:4996
67. Barnes AB, De Paëpe G, van der Wel PCA, Hu K-N, Joo C-G, Bajaj VS, Mak-Jurkauskas ML, Sirigiri JR, Herzfeld J, Temkin RJ, Griffin RG (2008) Appl Magn Reson 34:237
68. Maly T, Debelouchina GT, Bajaj VS, Hu K-N, Joo C-G, Mak-Jurkauskas ML, Sirigiri JR, van der Wel PCA, Herzfeld J, Temkin RJ, Griffin RG (2008) J Chem Phys 128:052211
69. Rosay M, Tometich L, Pawsey S, Bader R, Schauwecker R, Blank M, Borchard PM, Cauffman SR, Felch KL, Weber RT, Temkin RJ, Griffin RG, Maas WE (2010) Phys Chem Chem Phys (in press). doi:10.1039/c003685b
70. Van der Wel PCA, Hu K-N, Lewandowski J, Griffin RG (2006) J Am Chem Soc 128:10840

71. Barnes AB, Andreas LB, Huber M, Ramachandran R, van der Wel PCA, Veshtort M, Griffin RG, Mehta MA (2009) J Magn Reson 200:95
72. Bajaj VS, Mak-Jurkauskas ML, Belenky M, Herzfeld J, Griffin RG (2010) J Magn Reson 202:9
73. Bargon J, Fischer H (1967) Z Naturforsch 22a:1556
74. Ward HR, Lawler RG (1967) J Am Chem Soc 89:5518
75. Lawler RG (1967) J Am Chem Soc 89:5519
76. Bargon J (2006) Phys Chem Chem Phys 5:970
77. Cocivera M (1968) J Am Chem Soc 90:3261
78. Kaptein R, den Hollander JA, Antheunis D, Oosterhoff LJ (1970) J Chem Soc D 24:1687
79. Zysmilich MG, McDermott A (1994) J Am Chem Soc 116:8362
80. Schulten EAM, Matysik J, Alia, Kiihne S, Raap J, Lugtenburg J, Gast P, Hoff AJ, de Groot JM (2002) Biochemistry 41:8708
81. Roy E, Rohmer T, Gast P, Jeschke G, Alia A, Matysik J (2008) Biochemistry 47:4629
82. Diller A, Roy E, Gast P, van Gorkom HJ, de Groot HJM, Glaubitz C, Jeschke G, Matysik J, Alia A (2007) Proc Natl Acad Sci USA 104:12767
83. Daviso E, Prakash S, Alia A, Gast P, Neugebauer J, Jeschke G, Matysik J (2009) Proc Natl Acad Sci USA 106:22281
84. Walker T, Happer W (1997) Rev Mod Phys 69:629
85. Appelt S, Baranga B-A, Erickson CJ, Romalis MV, Young AR (1998) Phys Rev A 58:1412
86. Fink A, Baumer D, Brunner E (2005) Phys Rev A 72:053411
87. Ito T, Fraissard J (1982) J Chem Phys 76:5225
88. Raftery D, Long H, Meersmann T, Grandinetti PJ, Reven L, Pines A (1991) Phys Rev Lett 66:584
89. Bowers CR, Storhaug V, Webster CE, Bharatam J, Cottone A 3rd, Gianna R, Betsey K, Gaffney BJ (1999) J Am Chem Soc 121:9370
90. Locci E, Dehouck Y, Casu M, Saba G, Lai A, Luhmer M, Reisse J, Bartik K (2001) J Magn Reson 150:167
91. Rubin SM, Spence M, Goodson BM, Wemmer DE, Pines A (2000) Proc Natl Acad Sci USA 97:9472
92. Rubin SM, Lee S-Y, Ruiz EJ, Pines A, Wemmer DE (2002) J Mol Biol 322:425
93. Gröger C, Möglich A, Pons M, Koch B, Hengstenberg W, Kalbitzer HR, Brunner E (2003) J Am Chem Soc 125:8726
94. Dubois L, de Silva P, Landon C, Huber JG, Ponchet M, Vovelle F, Berthault P, Desvaux H (2004) J Am Chem Soc 126:15738
95. Anedda R, Era B, Casu M, Fais A, Ceccarelli M, Corda M, Ruggerone P (2008) J Phys Chem B 112:15856
96. Brunner E (1999) Conc Magn Reson 11:313
97. Raftery D (2006) Annu Rep NMR Spectrosc 57:205
98. Albert MS, Cates GD, Driehuys B, Happer W, Saam B, Springer CS Jr, Wishnia A (1994) Nature 370:199
99. Matsuoka S, Patz S, Albert MS, Sun Y, Rizi RR, Gefter WB, Hatabu H (2009) J Thorac Imaging 24:181
100. Brunner E, Seydoux R, Haake M, Pines A, Reimer JA (1998) J Magn Reson 130:145
101. Navon G, Song Y-Q, Rõõm T, Appelt S, Taylor RE, Pines A (1996) Science 271:1848
102. Desvaux H, Marion DJ, Huber G, Dubois L, Berthault P (2006) Eur Phys J Appl Phys 36:25
103. Schröder L, Lowery TJ, Hilty C, Wemmer DE, Pines A (2006) Science 314:446
104. Berthault P, Bogaert-Buchmann A, Desvaux H, Huber G, Boulard Y (2008) J Am Chem Soc 130:16456
105. Schlundt A, Kilian W, Beyermann M, Sticht J, Günther S, Höppner S, Falk K, Roetzschke O, Mitschang L, Freund C (2009) Angew Chem 121:4206
106. Bowers CR, Weitekamp DR (1986) Phys Rev Lett 57:2645
107. Eisenschmid TC, Kirss RU, Deutsch PP, Hommeltoft SI, Eisenberg R, Bargon J, Lawler RG, Balch AL (1987) J Am Chem Soc 109:8089
108. Pravica M, Weitekamp DP (1988) Chem Phys Lett 145:255
109. Korchak SE, Ivanov KL, Yurkovskaya AV, Vieth H-M (2009) Phys Chem Chem Phys 11:11146
110. Haake M, Natterer J, Bargon J (1996) J Am Chem Soc 118:8688
111. Kuhn LT, Bommerich U, Bargon J (2006) J Phys Chem A 110:3521
112. Carson PJ, Bowers CR, Weitekamp DP (2001) J Am Chem Soc 123:11821
113. Adams RW, Aguilar JA, Atkinson KD, Cowley MJ, Elliott PIP, Duckett SB, Green GGR, Khazal IG, López-Serrano J, Williamson DC (2009) Science 323:1708
114. Mishkovsky M, Frydman L (2008) Chemphyschem 9:2340
115. Wickramasinghe NP, Kotecha M, Samoson A, Past J, Ishii Y (2007) J Magn Reson 184:350
116. Linser R, Chevelkov V, Diehl A, Reif B (2007) J Magn Reson 189:209
117. Wickramasinghe NP, Parthasarathy S, Jones CR, Bhardwaj C, Long F, Kotecha M, Mehboob S, Fung LW-M, Past J, Samoson A, Ishii Y (2009) Nat Meth 6:215
118. Lopez JJ, Kaiser C, Asami S, Glaubitz C (2009) J Am Chem Soc 131:15970
119. Yamauchi K, Janssen JWG, Kentgens APM (2004) J Magn Reson 167:87
120. Kentgens APM, Bart J, van Bentum PJM, Brinkmann A, van Eck ERH, Gardeniers JGE, Janssen JWG, Knijn P, Vasa S, Verkuijlen MHW (2008) J Chem Phys 128:052202
121. Janssen H, Brinkmann A, van Eck ERH, van Bentum JM, Kentgens APM (2006) J Am Chem Soc 126:8722
122. Brinkmann A, Vasa SK, Janssen H, Kentgens APM (2010) Chem Phys Lett 485:275
123. Vasa SK, van Eck ERH, Janssen JWG, Kentgens APM (2010) Phys Chem Chem Phys 12:4813
124. Sakellariou D, Le Goff G, Jacquinot J-F (2007) Nature 447:694
125. Maricq MM, Waugh JS (1979) J Chem Phys 70:3300
126. Brunner E, Freude D, Gerstein BC, Pfeifer H (1990) J Magn Reson 90:90
127. Brunner E (1990) J Chem Soc Faraday Trans 86:3957
128. Samoson A, Tuherm T, Past J, Reinhold A, Anupõld T, Heinmaa I (2004) Top Curr Chem 246:15
129. Suwelack D, Rothwell WP, Waugh JS (1980) J Chem Phys 73:2559
130. Rothwell WP, Waugh JS (1981) J Chem Phys 74:2721
131. Fenzke D, Gerstein B, Pfeifer H (1992) J Magn Reson 98:469
132. van Rossum B-J, Boender GJ, de Groot HJM (1996) J Magn Reson A 120:274
133. Leskes M, Steuernagel S, Schneider D, Madhu PK, Vega S (2008) Chem Phys Lett 466:95
134. Lafon O, Wang Q, Hu B, Trébosc J, Deng F, Amoureux J-P (2009) J Chem Phys 130:014504
135. Chevelkov V, Rehbein K, Diehl A, Reif B (2006) Angew Chem Int Ed 45:3878
136. Akbey Ü, Lange S, Franks WT, Linser R, Rehbein K, Diehl A, van Rossum B-J, Reif B, Oschkinat H (2010) J Biomol NMR 46:67
137. Agarwal V, Linser R, Fink U, Faelber K, Reif B (2010) J Am Chem Soc 132:3187
138. Ashbrook SE (2009) Phys Chem Chem Phys 11:6892